Chemical Science

ROYAL SOCIETY OF CHEMISTRY

EDGE ARTICLE

View Article Online
View Journal | View Issue

Cite this: *Chem. Sci.*, 2023, **14**, 5116

All publication charges for this article have been paid for by the Royal Society of Chemistry

Received 21st February 2023
Accepted 16th April 2023

DOI: 10.1039/d3sc00975k

rsc.li/chemical-science

Conformationally supramolecular chirality prevails over configurational point chirality in side-chain liquid crystalline polymers†

Xiaoxiao Cheng,[a] Yijing Gan,[a] Gong Zhang,[a] Qingping Song,*[b] Zhengbiao Zhang *[a] and Wei Zhang *[ab]

In nature, the communication of primary amino acids in the polypeptides influences molecular-level packing, supramolecular chirality, and the resulting protein structures. In chiral side-chain liquid crystalline polymers (SCLCPs), however, the hierarchical chiral communication between supramolecular mesogens is still determined by the parent chiral source due to the intermolecular interactions. Herein, we present a novel strategy to enable the tunable chiral-to-chiral communication in azobenzene (Azo) SCLCPs, in which the chiroptical properties are not dominated by the configurational point chirality but by the conformationally supramolecular chirality that emerged. The communication of dyads biases supramolecular chirality with multiple packing preference, thereby overruling the configurational chirality of the stereocenter. The chiral communication mechanism between the side-chain mesogens is revealed through the systematic study of the chiral arrangement at the molecular level, including mesomorphic properties, stacking modes, chiroptical dynamics and further morphological dimensions.

Introduction

In nature, the most advanced functions of biological and non-biological systems emerge from homochiral primary structures,[1–3] such as DNA replication, enzyme asymmetric catalysis, and biological evolution.[4–6] The study of the chiral communication between primary structures can provide a theoretical basis for elucidating the origin of biological homochirality. Among this, artificial regulation of chiral communication in chiral polymeric supramolecules has been receiving ever-increasing attention due to its importance for both biological functions and application of chiral materials.[7,8] In particular, in side-chain liquid crystalline polymers (SCLCPs),[9–11] intensive research has been fueled by their actively tunable physicochemical properties and structural complexity, comparable to those of sophisticated natural materials.[12,13] However, the conventional chirality regulation of polymers mainly relies on the modification of the chiral stereocenter or the external chiral sources.[14–17] It is still a great challenge to regulate the chiral superstructures in different ways that can potentially program the helicity-switching in the opposite handedness.

In 1989, Green *et al.* first induced nonracemic main-chain helical polyisocyanates by a small chiral bias and described the unusual chirality amplification of the helical backbone. Two general strategies, Sergeants-and-Soldiers Principle (chiral-to-achiral communication) and Majority Rule (chiral communication between enantiomers), were established and further developed in helical systems with low helix inversion barriers.[18,19] Both effects are based on the accumulation of small local energy preferences in the helical main-chain, which results in an excess of helical conformation in completely dissolved polymer systems. In the case of an "abnormal" Sergeant-and-Soldiers effect,[20] Suginome *et al.* successfully controlled the helicity of poly(quinoxaline-2,3-diyl)s by modulating the contents of chiral/achiral dyads in the polymer chain. The backbone helicity could be inverted by changing the distribution between the chiral–chiral and the chiral–achiral segments according to the Sato model.[21] Furthermore, the combination of the chiral-sergeant and chiral-soldier dyads in the polymer chains could enable the selective interconversion of backbone helicity due to the differential expression of the two chiral components. This leads to pioneering exploration of chiral communication mechanisms, including chiral-to-chiral sergeants-and-soldiers effect,[22] chiral coalition,[23] chiral conflict,[24] chiral accord,[25] as well as synergistic chiral enhancement effect.[26]

Alternatively, modulating the stacking patterns of building blocks (*i.e.*, intra-chain and inter-chain packing, *J*- and *H*-aggregation according to Kasha's exciton theory[27]) is another efficient strategy for controlling the chiroptical properties and predicting the handedness of suprastructures.[28] Our previous studies described the multiple chiroptical inversion effects in SCLCP

[a]*State and Local Joint Engineering Laboratory for Novel Functional Polymeric Materials, Jiangsu Engineering Laboratory of Novel Functional Polymeric Materials, Suzhou Key Laboratory of Macromolecular Design and Precision Synthesis, College of Chemistry, Chemical Engineering and Materials Science, Soochow University, Suzhou, 215123, P. R. China. E-mail: zhangzhengbiao@suda.edu.cn; weizhang@suda.edu.cn*

[b]*School of Chemical and Environmental Engineering, Anhui Polytechnic University, Wuhu, 241000, P. R. China. E-mail: songqp@ahpu.edu.cn*

† Electronic supplementary information (ESI) available. See DOI: https://doi.org/10.1039/d3sc00975k

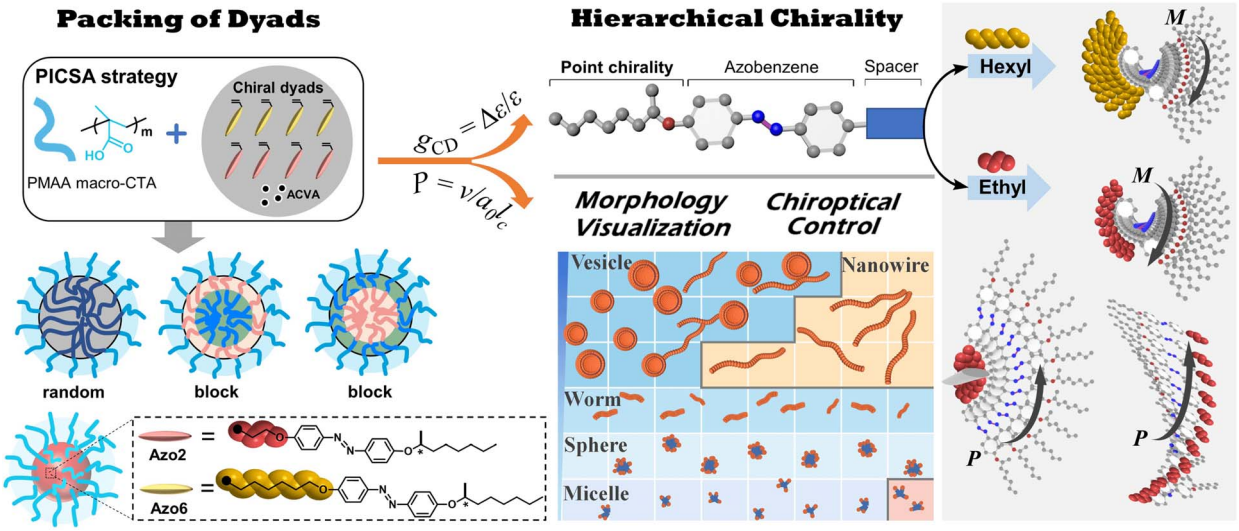

Scheme 1 The chiroptical control and morphological visualization in sequence-dependent SCLCPs. In these systems, the conformationally supramolecular chirality determines the chiroptical properties of the assemblies, regardless of the configurational point chirality of the stereocenter.

assemblies, which was driven by the transition of the different triple stacking modes (intra-chain stacking and inter-chain chiral transcription with the combination of *H*- and *J*-aggregation).[29,30] However, once two chiral building block dyads are packed into one polymer chain with different sequences (random or block with different distributions),[31–33] the synergistic effect of the supramolecular packing and the sequence switching will bring an unexpected chiral communication. Such a synergistic effect can guide the functional design of peptides, where the chiral communication of primary amino acid sequences in the polypeptides influences molecular-level packing, supramolecular chirality, and the resulting morphology.[34–36]

The elucidation of chiral communication in synthetic polymers is beneficial for the design of chiral materials, since the sequence of monomers in polymer chains can be easily regulated by living polymerization. Herein, we report the well-controlled chiral-to-chiral communication and morphological transition in SCLCP assemblies by copolymerizing two Azo dyads bearing the same stereocenter (Scheme 1). The relative ratio of the two chiral comonomer dyads, molecular weight of solvophobic blocks and the sequence of polymer structures have a significant effect on the chiral communication effect, resulting in tunable chiroptical properties of SCLCPs. This is collectively confirmed to be driven by multiple transitions of conformational supramolecular chirality in the chiral LC phase, ignoring the configuration of point chirality. The current sequence-controlled chiral communication strategy is different from typical chiral amplification effects in dissolved polymer systems, which do not involve stacking modes between chiral units.

Results and discussion

Polymerization-induced chiral self-assembly (PICSA) of amphiphilic supramolecular assemblies

To explore this unprecedented chiral communication, judicious choice of monomer dyads is thereby critical. Two chiral Azo comonomers, **Azo6** and **Azo2** (Scheme 1), with different spacers but the same chiral tails were chosen, as the former only underwent chiral head-to-head *H*-aggregation,[29] while the latter has been shown to undergo competitive DP-dependent stacking modes including intra-chain stacking, inter-chain *H*-aggregation and head-to-tail *J*-aggregation.[30]

We firstly synthesized solvophilic poly(methacrylic acid) as the macromolecular chain transfer agent (PMAA macro-CTA) by reversible addition–fragmentation chain transfer (RAFT) polymerization. The DP of PMAA macro-CTA was 51, the M_n and $Đ$ were 9000 g mol^{-1} and 1.08, according to ^{1}H NMR spectra and GPC analysis (Fig. S1†), respectively. The purified $PMAA_{51}$ macro-CTA was subsequently *in situ* chain-extended with **Azo2** and **Azo6** in selective ethanol. A series of amphiphilic $PMAA_{51}$-*b*-P(**Azo6**$_{1-n}$-*co*-**Azo2**$_n$), $PMAA_{51}$-*b*-P(**Azo6**$_{1-n}$-*b*-**Azo2**$_n$) and $PMAA_{51}$-*b*-P(**Azo2**$_n$-*b*-**Azo6**$_{1-n}$) copolymer assemblies composed of two chiral units in different ratios were prepared by the stepwise-feeding seeded RAFT polymerization (Fig. 1a and S2†). The conversion of the monomer was higher than 98%, and the linear M_n-conversion relationship (Fig. S3†) indicated the living nature of the polymerization-induced chiral self-assembly (PICSA) process.[37–40] Nearly quantitative polymerization was achieved and the polymer dispersity of all copolymer sequences was relatively low ($Đ$ < 1.25, Fig. S4–S6†). Their random and block distributions within the polymer chains were characterized by the Kelen–Tüdos method and ^{1}H NMR spectra.[41]

In the PICSA process, the living polymerization, supramolecular stacking and self-assembly occurred simultaneously, allowing the preparation of the corresponding supramolecular SCLCP assemblies *in situ*. Fig. 1 shows the aggregation-induced circular dichroism (CD) that originated from exciton coupling between the interacting Azo units in side-chains. It should be noted that the stereocenter is located at the terminal tails of the side-chain, which has a low influence on the radical polymerization of the flexible backbone. In this aspect, the introduced alkyl spacers also maintain the flexibility of the main-chains.

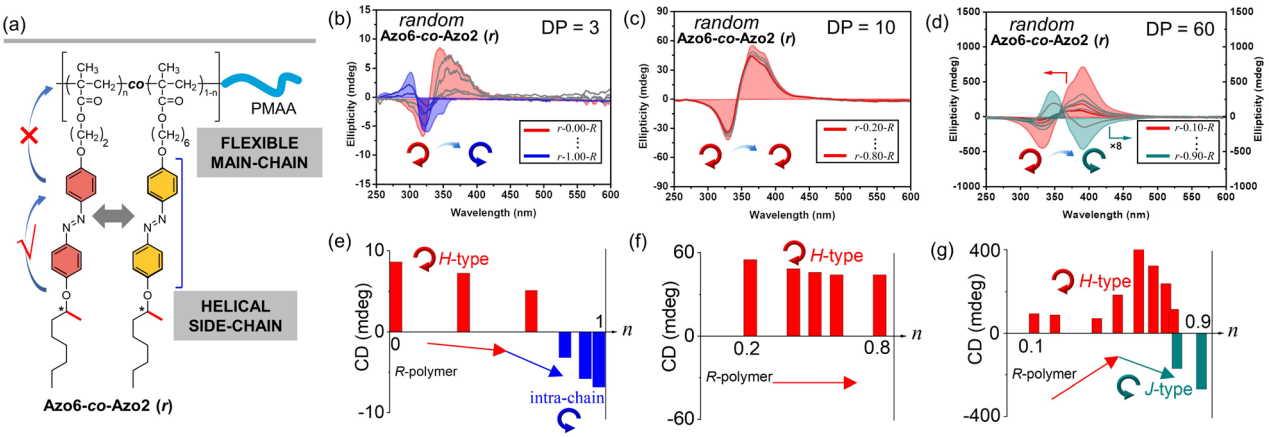

Fig. 1 (a) The chemical structures of random **Azo6-*co*-Azo2** SCLCP assemblies. CD spectra and maximum changes of random **Azo6-*co*-Azo2** assemblies with (b) and (e) DP = 3, (c) and (f) DP = 10, (d) and (g) DP = 60 with the increase of **Azo2** ratio (*n*).

The involved polymer contains four important units: (1) the main-chain of methacrylate; (2) alkyl spacer; (3) Azo mesogens and (4) alkyl chiral tails. A polymethacrylate main-chain was chosen because of its flexibility in polymers. The polymethacrylate main-chains were prepared by radical polymerization, whose tacticity is inherently not stereospecific. To preserve the flexibility of the main-chains, alkyl linkers were also inserted between the main-chain and the Azo mesogens. The induced supramolecular chirality arises from superstructural LC chirality, *i.e.*, helical structure *via* aggregation of side-chain Azo units, and is independent of the conformation of the polymer backbone.

The stacking modes of $PMAA_{64}$-*b*-$PAzo2MA_n^*$ diblock copolymer have been clearly revealed by many studies,[29,30,42] which are also presented in Fig. S7† for clarity. Broad bands containing four typical absorption peaks could be detected in the UV-vis spectra due to the aggregated interaction between adjacent azo units (Fig. S7a–e†). The local absorption maxima at *ca.* 320 nm, 340 nm, 357 nm and 377 nm can be assigned to the intra-chain stacking, inter-chain *H*-aggregation, non-associated Azo units and inter-chain *J*-aggregation, respectively. The type of supramolecular chirality can be determined by the dominated stacking modes by distinguishing the exciton coupling centers.

Chiroptical control by the synergistic effect of dyad ratios and sequence switching

CD, infrared spectroscopy (IR) and vibratory circular dichroism (VCD) were first employed to detect the conformation of the polymer backbone. As shown in Fig. S8,† CD signals of three copolymer sequences are obviously silent in the well-dissolved THF solvent. Meanwhile, three copolymer sequences exhibited same VCD silences of the C=O stretching band between 1750 and 1700 cm^{-1}. The results demonstrate that the polymer backbone does not have a distinct helical conformation. Thus, aggregation-induced LC chirality is responsible for CD signals of assemblies in ethanol dispersion. Taking Azo assemblies with an *R*-configuration as examples, random **Azo6-*co*-Azo2** SCLCP assemblies with DP = 3 showed a positive Cotton effect with a maximum at 347 nm when **Azo2** ratio $n = 0$ (Fig. 1b and e, inter-chain *H*-type). However, as *n* gradually increased to 1.0, the CD spectra gradually decreased and were opposite in sign with similar shapes but blue-shifted Cotton band (intra-chain stacking). The opposite sign indicates that the preferred helicity of the Azo stack inverts between $n = 0$ and $n = 1.0$. When the DP of the random copolymers was 10, little changes in the CD sign and shape can be observed as *n* gradually increased (Fig. 1c and f, inter-chain *H*-type). Unexpectedly, for copolymers with a DP of 60, the CD properties of the assemblies appear significantly different (Fig. 1d and g). For example, a positive Cotton effect was first observed when $n = 0.1$ (inter-chain *H*-type). As *n* gradually increased to 0.9, the CD maxima first increased and gradually decreased to nearly zero, and then inverted to negative values with a red-shifted Cotton band (inter-chain *J*-type). These transitions depend on the ratio of **Azo2** units, demonstrating that the **Azo2**/**Azo6** dyads compete for the chiral stacking in the self-assembly process.

The effect of the copolymer sequences on the chiral communication phenomena was then considered (Fig. 2a). As shown in Fig. 2b and c, the CD maxima of random **Azo6-*co*-Azo2**, block **Azo6-*b*-Azo2** and block **Azo2-*b*-Azo6** SCLCP assemblies were inverted twice and essentially dependent on the polymer sequences. Both chiral competition and sequence switching of Azo mesogens can change the hierarchical stacking modes and further control chiral-to-chiral communication in Azo side-chains (Fig. 2d). Therefore, we systematically investigated the dependence of chiroptical transitions on the Azo sequence, the ratio of **Azo2** units (*n*) and DP of Azo cores (Fig. 3 and S9–S12†).

We separately analyzed the results extracted from different sequence systems; all discussions were based on Azo assemblies with an *R*-configuration (blue line) unless otherwise specified. For the random **Azo6-*co*-Azo2** SCLCPs with Azo dyads randomly packed inside the core (Fig. 3a), the assemblies exhibited preferred positive g_{CD} values when DP = 3 and $n < 0.77$ (Fig. 3b, bottom). However, the positive signals were completely inverted to negative values when *n* approached 1.0. From a mechanistic

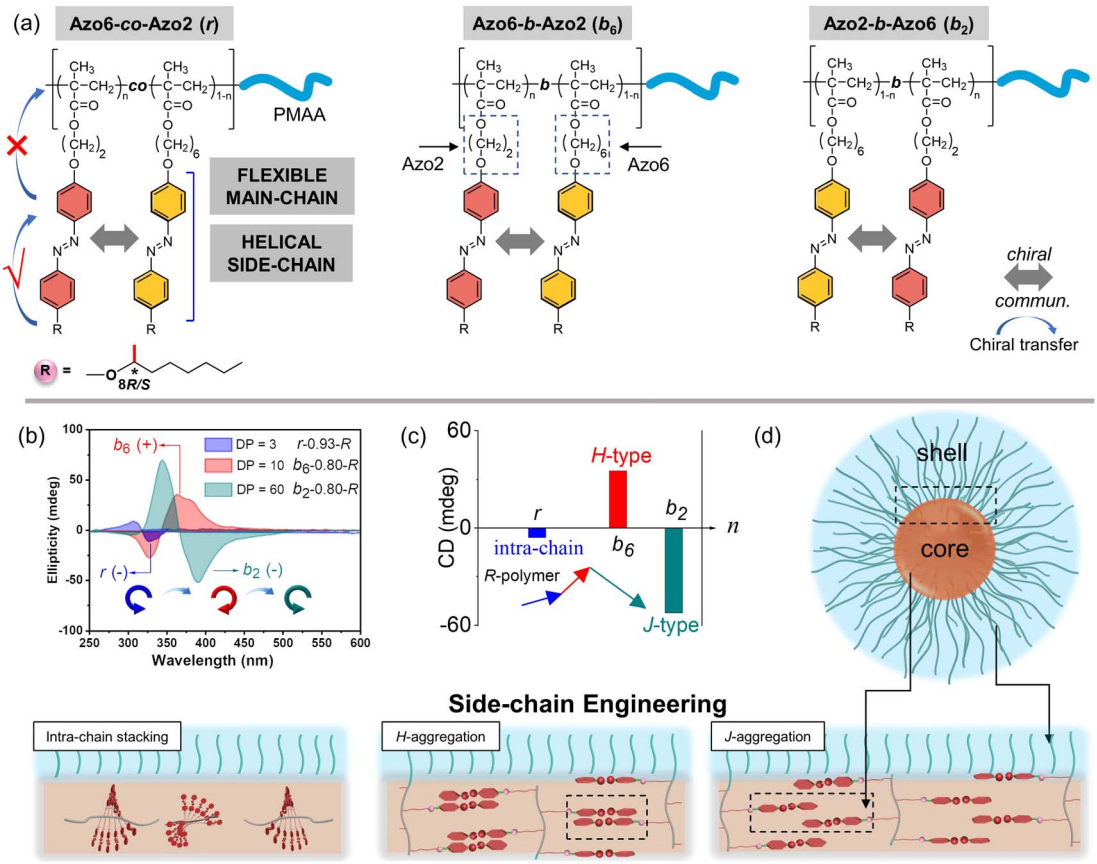

Fig. 2 Synergistic effects of chiral competition and sequence switching between Azo mesogens toward controlling the hierarchical chiral-to-chiral communication. (a) The chemical structures of random **Azo6-*co*-Azo2**, block **Azo6-*b*-Azo2** and block **Azo2-*b*-Azo6** copolymers. (b) and (c) CD spectra of random **Azo6-*co*-Azo2** (*r*, DP = 3, $n = 0.93$), block **Azo6-*b*-Azo2** (b_6, DP = 10, $n = 0.80$) and block **Azo2-*b*-Azo6** (b_2, DP = 60, $n = 0.80$). (d) Stacking modes inside the solvophobic core.

point of view, it should be noted that **Azo6** units only have chiral *H*-aggregation preference, while the **Azo2** unit can adopt changeable stacking modes with mutually inverted signals, such as π–π stacking along one polymer chain (intra-chain) or *H*- and *J*-aggregations of different polymer chains (inter-chain).[30] The chiroptical inversion probably originated from the transition from inter-chain *H*-aggregation to intra-chain stacking, according to the chiral competition of **Azo2**/**Azo6** dyads. For DPs of 10 and 20, the assemblies showed chiral *H*-aggregation without the chiroptical inversion, independent of the content of **Azo2** units. Interestingly, the chiroptical signals were inversed from positive to negative signals when the DP of the core-forming blocks was equal to 60 (Fig. 3b, top), with the reverse point *n* at 0.78, indicating the transition from *H*- to *J*-aggregates.

The ratio-dependent transition was also observed in block **Azo2-*b*-Azo6** SCLCP assemblies (Fig. 3c). When the DP was as low as 3 (Fig. 3d, bottom), the CD signals changed from positive to negative, indicating the transition from inter-chain *H*-aggregation to intra-chain stacking. The *H*-aggregates without reversal of g_{CD} values consistently existed in assemblies with a DP of 10. However, the *H*-to-*J* transformation-induced chiroptical inversion was found when the DP was 20. A continuous increase of DP to 60 still resulted in a *H*-to-*J* transition that varied with the **Azo2** ratio (Fig. 3d, top). The reversal points for DP20 and DP60 were $n = 0.39$ and 0.46, respectively. In this case, the **Azo6** unit that prefers *H*-packing is induced by the **Azo2** unit to arrange into a *J*-type stack, thereby inducing a reversal of g_{CD} values in the spectra.

For the block **Azo6-*b*-Azo2** SCLCP assemblies where the **Azo6** segment is adjacent to the PMAA fragment (Fig. 3e), the chiroptical inversion also existed when the DP of Azo core-forming blocks was 3 (Fig. 3f, bottom), the reversal point *n* was 0.77, similar to that of **Azo6-*co*-Azo2** and **Azo2-*b*-Azo6**. In contrast, the g_{CD} values showed the same *H*-aggregation associated with a positive Cotton effect when DP exceeded 10. This result indicated that the *H*-stacking of **Azo6** units commands the **Azo2** units to adopt the same stacking patterns, essentially independent of **Azo2** ratios and DP variation.

Meanwhile, the corresponding CD data also follow the changing tendency of g_{CD} values (Fig. S12†). Mirror-image chiroptical changes and therefore similar stacking transitions were presented in assemblies with an *S*-configuration, indicating the control over the differentiations of the chiral communication. According to the above results, the multiple inversions of the SCLCP assemblies are independent of the stereocenter, suggesting that chiroptical properties are dominated not by the

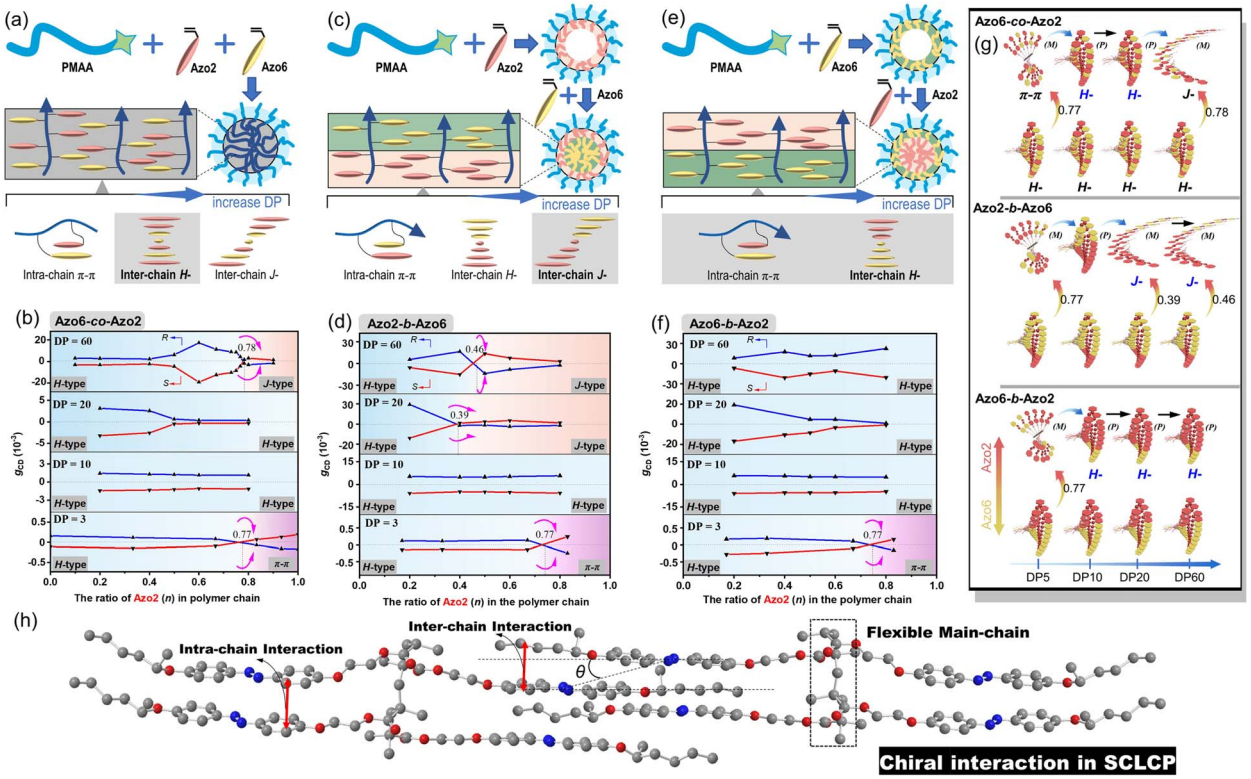

Fig. 3 Schematic representation of the PICSA procedure of (a) random **Azo6-*co*-Azo2**, (c) block **Azo2-*b*-Azo6** and (e) block **Azo6-*b*-Azo2** SCLCP assemblies. The g_{CD} values and the transition of stacking modes of (b) random **Azo6-*co*-Azo2**, (d) block **Azo2-*b*-Azo6**, (f) block **Azo6-*b*-Azo2** SCLCP assemblies with the increase of DP and **Azo2** ratios. (g) The internal stacking presented by the yellow **Azo6** and red **Azo2** units, respectively. (h) The homopolymer poly(**Azo2**) exhibits supramolecular polymorphism, and the unique asymmetric stacking modes can be depicted by the slip angle θ according to Kasha's exciton theory. (dissymmetry factors, $g_{CD} = \Delta\varepsilon/\varepsilon =$ [ellipticity/32 980]/absorbance at the CD extremum).

configurational point chirality but by the conformationally supramolecular chirality. The rich regulation of chiroptical properties in these SCLCP assemblies is impossible to realize in any previous main-chain helical polymers.

These multiple chiroptical inversions may follow a novel chiral-to-chiral communication mechanism, which is different from the traditional chiral communication effects (one is the chiral communication between the chiral sergeants and two enantiomeric soldiers, and the other is the classical "Sergeants-and-Soldiers Principle" composed of chiral sergeants and achiral soldiers). An explanation of those results can be envisioned by considering the chiral competition of the **Azo2** units in the helical *H*-packing of the parent poly(**Azo6**) segments and their response to the DP of Azo blocks (schematic presentation in Fig. 3g and h). The **Azo6** units tend to form a single preferred chiral *H*-aggregation. As a result, **Azo6** units can induce **Azo2** units to adopt preferential chiral *H*-aggregation in three sequences once small amounts of **Azo2** units are copolymerized, which is independent of the DP of Azo blocks. However, as the ratio of **Azo2** increased, the competition between **Azo2** and **Azo6** units that bias supramolecular helicity becomes more prominent; the more abundant **Azo2** units can command **Azo6** units to selectively adopt one of the three stacking modes. As a result, multiple chiroptical inversions can be observed in **Azo6-*co*-Azo2** and **Azo2-*b*-Azo6** SCLCP assemblies, although the transition of *H*- to *J*-aggregation occurs early in the latter. The block **Azo6-*b*-Azo2** SCLCP assemblies are exceptional since they possess no *J*-type chiroptical property. This can be ascribed to the preferential nucleation of first **Azo6** blocks, leading to the formation of thermodynamically stable *H*-aggregation. Thus, it is difficult for the second **Azo2** blocks to transform the already formed *H*-cores into unstable *J*-aggregates even at high DP and *n*. Therefore, we could conclude that the chiral communication mechanism observed in Azo SCLCPs is derived from two features: (1) the comonomers must display different packing preferences, *e.g.*, **Azo2** with different stacking modes in self-assembly and **Azo6** with only stable *H*-aggregation; (2) the SCLCP assemblies tend to express the chiroptical property of core-forming blocks that are firstly nucleated.

Helicity modulation and morphological visualization of polymer assemblies

The morphology of Azo assemblies may change due to the minimization of energetically unfavorable hydrophobe–solvent interactions.[43,44] The packing parameter P ($P = v/a_0 l_c$, a_0 is the area of the PMAA hydrophilic segment, v and l_c are the volume and length of the Azo hydrophobic segment) of amphiphilic Azo assemblies can be fine-tuned from $P \leq 1/3$ for spherical micelles

to $1/3 \leq P \leq 1/2$ for cylindrical micelles and then to $1/2 \leq P \leq 1$ for vesicles,[45–47] as the ratio of solvophobic **Azo6** units and the DP of the core-forming blocks increased. The morphological transition of these Azo SCLCP assemblies was further analyzed (Fig. 4 and S13–S16†). Taking assemblies with DP = 60 as an example (*R*-configuration), random **Azo6-*co*-Azo2** assemblies gradually changed from vesicles to long nanowires as the ratio of **Azo2** units increased (Fig. 4a). The average diameter $\bar{d}$ obtained from TEM first increased from 266 to 516 nm, and then decreased to 32 nm. This morphological transition was also observed in the case of block **Azo2-*b*-Azo6** assemblies (Fig. 4b), while the $\bar{d}$ continuously decreased from 187 to 34 nm. Interestingly, the inner stacking modes of these two sequences also changed from *H*-aggregation to *J*-aggregation when the vesicles were completely transformed into nanowires. Meanwhile, strong attenuation and reverse of CD signals from *H*-to-*J* transition were observed when vesicles were completely transformed into long nanowires (CD values in Fig. 4a and b). The CD changes can be ascribed to that the uniform helical twisting in smectic layers is forbidden by symmetry rules. The *H*-aggregates would first grow together with the orthogonal smectic layers (*vide infra*), inducing strong *H*-stacking helical bias, which would be then suppressed since the smectic layers become more ordered. Interestingly, the vesicular morphology of block **Azo6-*b*-Azo2** assemblies was retained in all cases without morphological transition (Fig. 4c), which is consistent with the fact that only *H*-aggregated signals were observed in the CD spectra.

Clearly, tuning the ratio of **Azo2** units in polymer chains and thus the sequences of the resultant random or block copolymers effectively varies the morphologies of the assemblies. For SCLCP assemblies with identical DPs (DP = 60) and **Azo2** ratios ($n = 0.8$) (red boxes in panels Fig. 4a–c), the sequence switching-driven morphological transition was further confirmed by AFM measurements (Fig. 4d and S16†). Exclusively left-handed (*M*-type) helical nanowires were observed both in random **Azo6-*co*-Azo2** and block **Azo2-*b*-Azo6** assemblies with an *R*-configuration, corresponding to the negative Cotton effect of *J*-aggregates. Meanwhile, isotropic vesicles of block **Azo6-*b*-Azo2** were observed in the AFM images, and the corresponding CD values

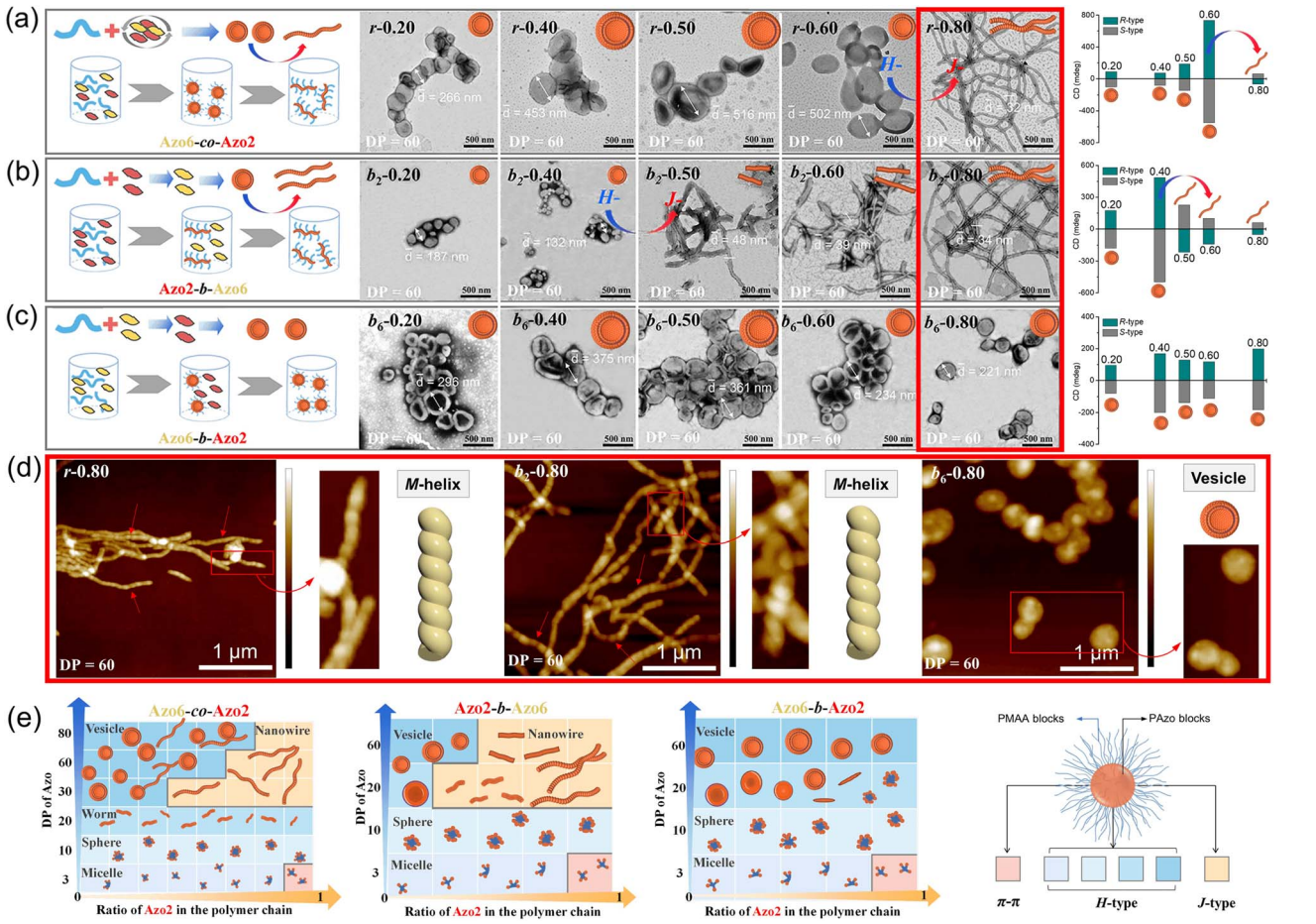

Fig. 4 Solvophobic phase separation drives sharp morphological changes of assemblies with different **Azo2** ratios. (a) Random **Azo6-*co*-Azo2** (*r*), (b) block **Azo2-*b*-Azo6** (b_2) and (c) block **Azo6-*b*-Azo2** (b_6) of Azo assemblies with an *R*-configuration. (d) AFM images corresponding to samples shown in the red box of (a), (b) and (c), respectively. (e) Phase diagram of the self-assembled morphology with different DP and **Azo2** unit ratios in these copolymer sequences. The packing modes are shown with gradated background colors representing intra-chain stacking (pink), inter-chain *H*-aggregation (blue) and *J*-aggregation (orange).

displayed positive signals related to *H*-aggregation. Considering the sequences of polymers was the only alteration in these SCLCPs; it was reasonable to infer that the morphological differences as well as above chiroptical changes were attributed to the sequence switching.

The growing DP of Azo core-forming blocks leads to an increase in the packing parameter *P*, thus a micelle-to-sphere-to-vesicle transition was observed for these SCLCP assemblies (Fig. 4e). The phase diagrams clearly showed preferential morphological transitions at a lower **Azo2** ratio, regardless of the polymer sequences. However, the inner stacking modes are closely related to the morphological transition of the assemblies. For example, the packing mode of intra-chain stacking only existed in micelles (pink area). The change from vesicles to nanowires appeared in both **Azo6-*co*-Azo2** and **Azo2-*b*-Azo6** due to the transition from *H*-aggregation (blue area) to *J*-aggregation (orange area), whereas the vesicle is the main phase in **Azo6-*b*-Azo2**; in this case, only *H*-aggregates are present. Therefore, both the chiral communication and morphology visualization of SCLCP assemblies can be achieved through the transition of the conformationally supramolecular chirality of the Azo building blocks.

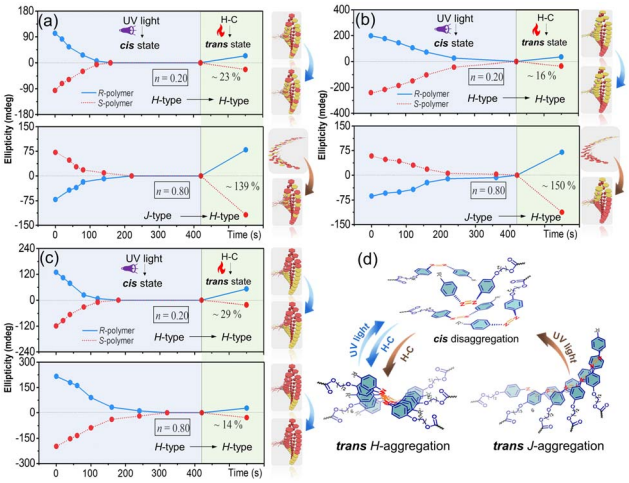

Fig. 5 Changes of the CD maximum (first Cotton band) of Azo SCLCP assemblies upon 365 nm UV light irradiation and H–C treatment. (a) Random **Azo6-*co*-Azo2**, (b) block **Azo2-*b*-Azo6** and (c) block **Azo6-*b*-Azo2** with $n = 0.2$ and $n = 0.8$, respectively. (d) The helical order–disorder transition of *H*- and *J*-aggregations in the process of *trans*–*cis*–*trans* isomerization. The DP of the corresponding Azo core-forming blocks is 60.

Dynamic chiral response controlled by UV/vis light and temperature

The conformational supramolecular chirality can be further regulated by external stimuli due to the nature of weak noncovalent interactions and the flexible *trans*–*cis* properties of Azo units.[48–52] Herein, light and temperature were employed to switch the handedness of the helical structures. When the Azo assemblies are exposed to 365 nm UV light, significant decreases of the π–π* transition (*ca.* 350 nm) as well as increases of the n–π* transition (*ca.* 450 nm) were detected, regardless of the copolymer sequences and stacking modes (Fig. S17 and S18†). The CD values of both *H*- and *J*-aggregates decreased during the *trans*-to-*cis* processes (Fig. 5a–c), which completely disappeared in the photostationary state due to the loss of ordered helical suprastructures. The bent *cis*-form Azo units with various (Ph-N=N-Ph) dihedral angles disrupted the efficient Azo helical stacks and led to disordered structures (Fig. 5d).

In the heating–cooling (H–C) assisted reassembly process, the destroyed Azo stacks in these copolymer assemblies underwent different pathways to recover their helical superstructures, as demonstrated by the reappearance of the CD signals. After heating and then cooling **Azo6-*co*-Azo2** assemblies, recovery effectiveness of ~23% for the $H \rightarrow H$ pathway was observed when $n = 0.20$ (Fig. 5a, top), while a chiroptical inversion of the $J \rightarrow H$ pathway with ~139% chiroptical enhancement was detected when $n = 0.80$ (Fig. 5a, bottom). Analogous H–C treatment of **Azo2-*b*-Azo6** showed similar trends to that of **Azo6-*co*-Azo2**, with recovery effectiveness of ~16% for the $H \rightarrow H$ pathway and ~150% enhancement for the $J \rightarrow H$ pathway (Fig. 5b). Nevertheless, only the $H \rightarrow H$ pathway with ~29% ($n = 0.20$) and ~14% ($n = 0.80$) recovery effectiveness was observed in **Azo6-*b*-Azo2** (Fig. 5c). These results indicate that *H*-aggregates are more thermodynamically stable than *J*-aggregates (Fig. 5d). When *cis*-disaggregated Azo units recover to *trans* helical stacks, the H–C procedure could invert and enhance the helical asymmetry in the $J \rightarrow H$ transition while inhibiting the recovery of helical asymmetry in the $H \rightarrow H$ process. The effectiveness of the chiral recovery depends on the sequence differences and the chiral competition between **Azo2**/**Azo6** dyads for generating the preferred noncovalent stacks.

Driving force and communication mechanism of chirality evolution

To investigate the underlying chiral communication mechanism, the changes in the mesomorphic properties and inner packing parameters of Azo copolymers were studied in detail. Our previous results demonstrated that the chirality of intra-chain stacking is dominant in the amorphous phase, while *H*-chirality and *J*-chirality are dominant in TGBA* and SmA* phases, respectively.[30] For the assemblies containing intra-chain stacking, as shown in Fig. S19–S21,† only broad peaks with a normal distribution ($2\theta = 16.0°$) were observed by wide-angle X-ray diffraction (WAXD) in the angle region where LC structures were expected. And no scattering peaks were detected in small-angle X-ray scattering (SAXS) patterns (Fig. S22–S24†), suggesting the amorphous nature of Azo assemblies with intra-chain stacking mode. The typical distance between intra-chain adjacent Azo units in chiral π–π stacking mode is 3.6 Å.

Meanwhile, Azo assemblies with chiroptical properties of *H*- and *J*-aggregation modes showed a clear LC phase with periodic layered structures, regardless of the copolymer sequences. These can be distinguished by the clear diffraction peaks in WAXD patterns (Fig. S19–S21†) and two proportional scattering peaks in SAXS spectra ($q_1/q_2 = 1/2$, Fig. S22–S24†). The periodicity of layer spacing (d) and the distance of Azo units (r) were calculated according to SAXS and WAXD patterns, as presented in Fig. 6a and

b. With the increase of **Azo2** units, the layer spacing *d* decreased from *ca.* 5.5 nm to *ca.* 4.8 nm (Fig. 6a), but was less than twice of the fully extended **Azo6** and **Azo2** chain length (2 L = 5.88 nm for **Azo6** and 2 L = 4.94 nm for **Azo2** calculated by Gaussian 09, Fig. 6c). These results clearly suggested a double-layered smectic structure with an interdigitation of the side-chains.

In the LC phase, however, the distances of Azo units (*r*) increased with the increase of **Azo2** units (Fig. 6b). Because **Azo2** units with a shorter spacer have a weaker solvophobicity than **Azo6** units, as the ratio of **Azo2** units increased, the loosed microdomains and increased distances lead to a smaller slip angle θ of Azo units (Fig. 6c), resulting in the transition from *H*-aggregation (θ > magic angle 54.7°) to *J*-aggregation (θ < 54.7°). POM images also indicated the LC phase transition in three copolymer sequences, where the bright LC aggregates can be observed in a broad region (Fig. S25–S27†). The amorphous-to-TGBA*-to-SmA* phase transition allows the transition of three stacking modes, resulting in the mutually opposite chiroptical properties of exciton coupling between closely situated transition dipole moments on neighboring Azo units.

As a result, the LC phase structures and chiroptical transitions were dependent on the copolymer sequences (Fig. 6d). In **Azo6-*co*-Azo2** and **Azo2-*b*-Azo6**, the preferential nucleation of **Azo2** units allows phase transitions to occur, so multiple chiroptical inversions of the three stacking modes exist. For example, in **Azo2-*b*-Azo6**, the stepwise-feeding procedure favors the first **Azo2** segment to form the SmA* phase before adding the second **Azo6** segment. As a result, the chiroptical inversion from *H*- to *J*-aggregation occurs favorably, which can be reflected by the CD signal reversal at DP = 20 and *n* = 0.39.

In **Azo6-*b*-Azo2**, however, the **Azo6** segments tend to adopt a preferred TGBA* phase responsible for inducing a solely chiral *H*-aggregation in the nucleus. Thus, the pre-formed *H*-aggregates of **Azo6** units dominate the chiral preference of the core and command the neighbouring **Azo2** units to adopt the same *H*-aggregation. As a result, the transition from *H*- to *J*-aggregation did not occur in these copolymer assemblies even at higher DP and *n*, as demonstrated by CD in Fig. 3f.

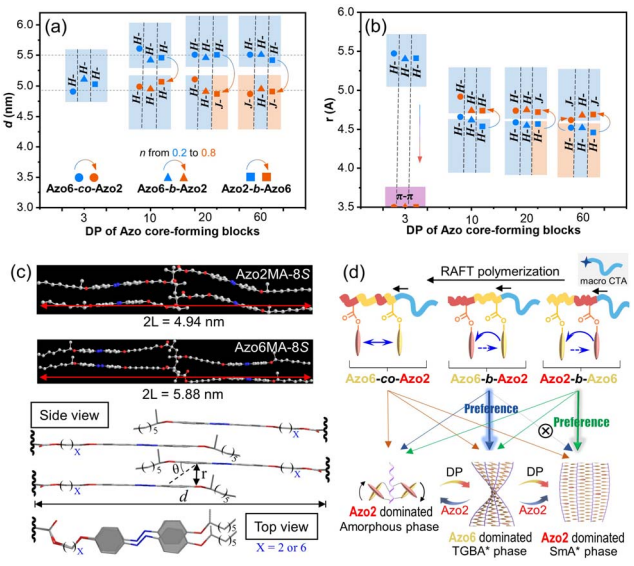

Fig. 6 The mesomorphic properties and inner packing parameters in the Azo copolymer series. Plots of (a) the calculated layer spacing (*d*) and (b) the distances of Azo units (*r*) *versus* DP of Azo core-forming blocks (the increase of **Azo2** ratio is presented as a color change from blue dots: *n* = 0.2 to red dots: *n* = 0.8). (c) The fully extended length of the **Azo2**MA-8*S* and **Azo6**MA-8*S* side-chains. Bottom: the proposed packing structures of the double-layered LC phase in the Azo SCLCP series. (d) Relationship between copolymer sequences and competitive phase transitions.

Conclusions

In summary, we have reported the regulation of conformationally supramolecular chirality in SCLCP assemblies composed of random **Azo6-*co*-Azo2**, block **Azo2-*b*-Azo6** and block **Azo2-*b*-Azo6**, in which the chiral dyads possess the same configurational point chirality. Sequence switching can generate differences in the stacking preference and aggregation order of **Azo2**/**Azo6** units, enabling control of the chiral-to-chiral communication and assembly morphologies. The ratio- and DP-dependent chiroptical properties and LC characterization indicate that the transition of mesomorphic properties, for example, the amorphous-to-TGBA*-to-SmA* phase transition, is the driving force for the chiral communication effect. Moreover, a multidimensional phase diagram from micelles to spheres, worms, helical nanowires and vesicles was observed, visually demonstrating the transition of the stacking modes. The helicity modulation and morphology visualization of SCLCP are achieved through the transition of the conformational supramolecular arrangements, which breaks the limitation of absolute configuration and will find practical application in the design of functions in complex LC materials.

Data availability

The experimental data can be found in the ESI† and manuscript and is referred to throughout the manuscript.

Author contributions

Prof. W. Zhang and X. X. Cheng conceived the research idea and co-wrote the original draft. Y. J. Gan, Q. P. Song and G. Zhang performed the synthesis and characterization. Prof. W. Zhang and Prof. Z. B. Zhang revised the final manuscript.

Conflicts of interest

There are no conflicts to declare.

Acknowledgements

The authors are grateful for the financial support from the National Nature Science Foundation of China (92056111, 21971180 and 21925107), China Postdoctoral Science Foundation (2022M722312), Key Laboratory of Polymeric Material Design and Synthesis for Biomedical Function, the Priority

Academic Program Development (PAPD) of Jiangsu Higher Education Institutions and the Program of Innovative Research Team of Soochow University.

Notes and references

1 Y. Ma, X. Cheng, H. Ma, Z. He, Z. Zhang and W. Zhang, *Chem. Sci.*, 2022, **13**, 13623–13630.
2 T. Ikai, M. Okubo and Y. Wada, *J. Am. Chem. Soc.*, 2020, **142**, 3254–3261.
3 J. Yuan, X. Lu, Q. Li, Z. Lu and Q. Lu, *Angew. Chem., Int. Ed.*, 2021, **60**, 12308–12312.
4 T. Miao, X. Cheng, H. Ma, Z. He, Z. Zhang, N. Zhou, W. Zhang and X. Zhu, *Angew. Chem., Int. Ed.*, 2021, **60**, 18566–18571.
5 T. Nakano and Y. Okamoto, *Chem. Rev.*, 2001, **101**, 4013–4038.
6 S. Cai, J. Chen, S. Wang, J. Zhang and X. Wan, *Angew. Chem., Int. Ed.*, 2021, **60**, 9686–9692.
7 W. Shang, X. Zhu, Y. Jiang, J. Cui, K. Liu, T. Li and M. Liu, *Angew. Chem., Int. Ed.*, 2022, **61**, e202210604.
8 Y. Yan, K. Deng, Z. Yu and Z. Wei, *Angew. Chem., Int. Ed.*, 2009, **48**, 2003–2006.
9 T. Miao, X. Cheng, G. Zhang, Y. Wang, Z. He, Z. Wang and W. Zhang, *Chem. Sci.*, 2023, **14**, 1673–1678.
10 L. Wang, L. Yin, W. Zhang, X. Zhu and M. Fujiki, *J. Am. Chem. Soc.*, 2017, **139**, 13218–13226.
11 Z. Zheng, Y. Li, H. K. Bisoyi, L. Wang, T. J. Bunning and Q. Li, *Nature*, 2016, **531**, 352–356.
12 C. D. H. Alarcon, S. Pennadam and C. Alexander, *Chem. Soc. Rev.*, 2005, **34**, 276–285.
13 J. Babin, M. Pelletier, M. Lepage, J.-F. Allard, D. Morris and Y. Zhao, *Angew. Chem., Int. Ed.*, 2009, **48**, 3329–3332.
14 H. Goto and E. Yashima, *J. Am. Chem. Soc.*, 2002, **124**, 7943–7949.
15 T. Ikai, R. Ishidate, K. Inoue, K. Kaygisiz, K. Maeda and E. Yashima, *Macromolecules*, 2020, **53**, 973–981.
16 G. Liu, X. Li, J. Sheng, P. Z. Li, W. K. Ong, S. Z. F. Phua, H. Agren, L. Zhu and Y. Zhao, *ACS Nano*, 2017, **11**, 11880–11889.
17 K. Maeda, S. Wakasone, K. Shimomura, T. Ikai and S. Kanoh, *Macromolecules*, 2014, **47**, 6540–6546.
18 M. M. Green, M. P. Reidy, R. J. Johnson, G. Darling, D. J. Oleary and G. Willson, *J. Am. Chem. Soc.*, 1989, **111**, 6452–6454.
19 M. M. Green, N. C. Peterson, T. Sato, A. Teramoto, R. Cook and S. Lifson, *Science*, 1995, **268**, 1860–1866.
20 Y. Nagata, T. Nishikawa and M. Suginome, *J. Am. Chem. Soc.*, 2015, **137**, 4070–4073.
21 S. Wang, J. Chen, X. Feng, G. Shi, J. Zhang and X. Wan, *Macromolecules*, 2017, **50**, 4610–4615.
22 K. Cobos, E. Quinoa, R. Riguera and F. Freire, *J. Am. Chem. Soc.*, 2018, **140**, 12239–12246.
23 S. Arias, R. Rodriguez, E. Quinoa, R. Riguera and F. Freire, *J. Am. Chem. Soc.*, 2018, **140**, 667–674.
24 M. Alzubi, S. Arias, R. Rodriguez, E. Quinoa, R. Riguera and F. Freire, *Angew. Chem., Int. Ed.*, 2019, **58**, 13365–13369.
25 S. Sforza, T. Tedeschi, R. Corradini and R. Marchelli, *Eur. J. Org. Chem.*, 2007, 5879–5885.
26 K. Cobos, R. Rodriguez, E. Quinoa, R. Riguera and F. Freire, *Angew. Chem., Int. Ed.*, 2020, **59**, 23724–23730.
27 G. Liu, J. Sheng, H. Wu, C. Yang, G. Yang, Y. Li, R. Ganguly, L. Zhu and Y. Zhao, *J. Am. Chem. Soc.*, 2018, **140**, 6467–6473.
28 F. Yang, X. Liu and Z. Yang, *Angew. Chem., Int. Ed.*, 2021, **60**, 14671–14678.
29 X. Cheng, T. Miao, L. Yin, Y. Ji, Y. Li, Z. Zhang, W. Zhang and X. Zhu, *Angew. Chem., Int. Ed.*, 2020, **59**, 9669–9677.
30 X. Cheng, T. Miao, Y. Ma, X. Zhu, W. Zhang and X. Zhu, *Angew. Chem., Int. Ed.*, 2021, **60**, 24430–24436.
31 L. Wang, Y. Ding, Q. Liu, Q. Zhao, X. Dai, X. Lu and Y. Cai, *ACS Macro Lett.*, 2019, **8**, 623–628.
32 R. K. Roy and J. F. Lutz, *J. Am. Chem. Soc.*, 2014, **136**, 12888–12891.
33 T. Wen and R. Ho, *ACS Macro Lett.*, 2017, **6**, 370–374.
34 E. G. Bellomo, M. D. Wyrsta, L. Pakstis, D. J. Pochan and T. J. Deming, *Nat. Mater.*, 2004, **3**, 244–248.
35 D. Ke, C. Zhan, A. D. Li and J. Yao, *Angew. Chem., Int. Ed.*, 2011, **50**, 3715–3719.
36 N. R. Lee, C. J. Bowerman and B. L. Nilsson, *Biomacromolecules*, 2013, **14**, 3267–3277.
37 C. E. Boott, J. Gwyther, R. L. Harniman, D. W. Hayward and I. Manners, *Nat. Chem.*, 2017, **9**, 785–792.
38 J. Chen, S. Cai, R. Wang, S. Wang, J. Zhang and X. Wan, *Macromolecules*, 2020, **53**, 1638–1644.
39 S. Jimaja, S. Varlas, Y. Xie, J. C. Foster, D. Taton, A. P. Dove and R. K. O'Reilly, *ACS Macro Lett.*, 2020, **9**, 226–232.
40 F. Lv, Z. An and P. Wu, *Nat. Commun.*, 2019, **10**, 1397.
41 K. Maeda, M. Muto, T. Sato and E. Yashima, *Macromolecules*, 2011, **44**, 8343–8349.
42 G. Iftime, F. L. Labarthet, A. Natansohn and P. Rochon, *J. Am. Chem. Soc.*, 2000, **122**, 12646–12650.
43 J. Yeow and C. Boyer, *Adv. Sci.*, 2017, **4**, 1700137.
44 B. Zhang, X. Lv, A. Zhu, J. Zheng, Y. Yang and Z. An, *Macromolecules*, 2018, **51**, 2776–2784.
45 R. Deng, M. J. Derry, C. J. Mable, Y. Ning and S. P. Armes, *J. Am. Chem. Soc.*, 2017, **139**, 7616–7623.
46 M. Douverne, Y. Ning, A. Tatani, F. C. Meldrum and S. P. Armes, *Angew. Chem., Int. Ed.*, 2019, **58**, 8692–8697.
47 S. Xu, J. Yeow and C. Boyer, *ACS Macro Lett.*, 2018, **7**, 1376–1382.
48 J. del Barrio, R. M. Tejedor, L. S. Chinelatto, C. Sanchez, M. Pinol and L. Oriol, *J. Mater. Chem.*, 2009, **19**, 4922–4930.
49 S. Huang, Y. Chen, S. Ma and H. Yu, *Angew. Chem., Int. Ed.*, 2018, **57**, 12524–12528.
50 Y. J. Gan, H. B. Dai, Y. F. Ma, X. X. Cheng, Z. Wang and W. Zhang, *Macromolecules*, 2022, **55**, 8556.
51 Z. Liu, Y. Yao, X. Tao, J. Wei and S. Lin, *ACS Macro Lett.*, 2021, **10**, 1174–1179.
52 X. Tong, L. Cui and Y. Zhao, *Macromolecules*, 2004, **37**, 3101–3112.